Non-Boussinesq effects in free thermal convection

Xiao-Zhong Wu and Albert Libchaber
The Department of Physics and the Research Institutes, The University of Chicago, 5640 South Ellis Avenue, Chicago, Illinois 60637
(Received 17 July 1990)

Non-Boussinesq effects in a Rayleigh-Bénard convection system lead to a symmetry breaking between the top and the bottom boundary layers. We have found that the two layers adjust their temperature drops and the thicknesses λ such that their temperature scales $\nu\kappa/g\alpha\lambda^3$ are equal, where α is the thermal expansion coefficient, g is the gravitational acceleration, and ν and κ are the kinematic viscosity and thermal diffusivity, respectively.

I. INTRODUCTION

In most of the studies of thermal convection, the Oberbeck-Boussinesq[1,2] (OB) approximation has been assumed; i.e,. the temperature dependence of all the fluid properties other than the fluid density are considered constant. This approximation simplifies the convection problem greatly. However, there are cases where this approximation is no longer valid, hence it is natural to study how it influences the experimental results. Furthermore, since the symmetry between the top (colder) and bottom (hotter) boundary layers is broken, some relations, which are hidden in the OB case, may be revealed. This in turn may shed some light on the OB case.

When the Rayleigh number R is less than 10^3, the heat is transported by conduction. In this case, the temperature profile, heat flux, etc., can be calculated analytically from the diffusion equation. When the convection starts, the situation becomes nontrivial. A few researchers[3-10] have studied the non-OB effects near the onset of convection. However, as the flow in the convection cell reaches a different turbulence state, non-OB effects may have different behaviors. In this paper we shall discuss the non-OB effects in hard turbulence[11] ($R > 10^7$), far above the onset of convection.

In Sec. II of this paper, we shall briefly describe the experimental setup and procedures. The situation where the non-OB effects appear is explained. In Sec. III, we present the experimental results, such as the asymmetry of the two boundary layers, the strange behavior of the Nusselt number, and the rms temperature fluctuations. Finally, in Sec. IV, we discuss three different models. Since the equations available are not enough to determine uniquely the temperature drops and the thicknesses of the two boundary layers, one more relation has to be proposed. We discuss the equality of the Rayleigh numbers, the equality of the velocity scales, and the equality of the temperature scales, for the two boundary layers. The last one is provied to be the best experimentally. The consequences of the last model are discussed and compared with the experimental results.

II. EXPERIMENT

We have performed the low-temperature helium-gas convection experiment in three different vertical cylindrical cells, with diameters 8.7, 20, and 20 cm, heights 8.7, 40, and 3 cm, thus aspect ratio 1, 0.5, and 6.7, respectively. Of these three cells, the one of the largest aspect ratio, diameter 20 cm and height 3 cm, has the best temperature regulation. Thus we shall focus on this cell in this paper. The cell sidewall is 2-mm-thick stainless steel. The sidewall heat transport is of the same order of magnitude as the heat conducted by the gas, thus much smaller than the heat transported by convecting gas. Both the top and bottom plates are made from oxygen-free high-conductivity copper. The bottom plate has a thickness of 2.0 cm and the top plate of 6.4 cm. GR-200A germanium resistance temperature sensors from the Lake Shore Cryotronics, Inc., are used to measure the temperatures of the plates. At 5 K, their typical resistance is around 1.5 kΩ, and the sensitivity is about 1 mK/Ω. They are embedded in both plates, several millimeters away from the inner surfaces. The method of measuring the thermometers, as well as the local temperature bolometers in the fluid, has been described in Ref. 12. The entire cell is in a vacuum jacket with its top plate in thermal contact with a liquid-helium bath. The top plate is regulated at a given temperature around 5 K. The top-plate temperature fluctuation is a fraction of 1 mK for low Rayleigh numbers and can reach a few mK for the highest Rayleigh numbers. When not heating the bottom plate, the temperature difference of the two plates is not zero and increases slightly with the top-plate temperature, but the maximum difference is less than 5 mK. We think that this difference is due to the imperfect vacuum. By applying a constant dc heat to the bottom plate, a temperature drop Δ is imposed. The cell is filled with helium gas of various densities. The density of the gas is computed by measuring the equilibrium pressure with an absolute pressure transductor of MKS Instruments, Inc., and the temperature of both plates. The fluid properties and the relations are based on the equations and tables given by McCarty,[13,14] who has reviewed most of the works on helium-gas properties.

The control parameter of this experiment is the Rayleigh number

$$R = \frac{\alpha g L^3 \Delta}{\nu\kappa} , \tag{1}$$

where α is the thermal expansion coefficient, g is the

TABLE I. Experimental values of the Rayleigh number R; Nusselt number N; temperature difference Δ; the ratio of the temperature drops across the top and bottom boundary layers x; and the fluid properties in central region c, top t, and bottom b boundary layers.

R	N	Δ (mK)	x	ρ (10^{-2} g/cm^3)	Region	T (K)	α (1/K)	ν (10^{-4} cm^2/s)	κ (10^{-4} cm^2/s)	χ (mW/cmK)
					c	4.486	0.267	29.1	41.4	0.0954
2.10×10^{8}	35.7	357	0.89	0.406	t	4.402	0.274	28.0	39.7	0.0939
					b	4.581	0.259	30.3	43.4	0.0970
					c	4.469	0.339	14.1	17.6	0.0990
5.75×10^{8}	47.7	158	0.87	0.870	t	4.432	0.345	13.8	17.1	0.0985
					b	4.511	0.331	14.4	18.1	0.0996
					c	4.553	0.329	14.3	17.9	0.100
1.21×10^{9}	59.2	356	0.87	0.870	t	4.469	0.343	13.7	17.0	0.0993
					b	4.648	0.314	15.0	19.1	0.102
					c	4.723	0.440	8.90	9.13	0.110
5.13×10^{9}	92.7	358	0.85	1.53	t	4.633	0.479	8.44	8.35	0.110
					b	4.812	0.409	9.35	9.90	0.111
					c	4.747	0.499	7.92	7.49	0.114
3.35×10^{9}	86.5	150	0.89	1.76	t	4.712	0.519	7.75	7.21	0.114
					b	4.787	0.478	8.12	7.84	0.114
					c	4.725	0.507	7.87	7.41	0.113
8.42×10^{9}	105	366	0.79	1.76	t	4.644	0.559	7.48	6.72	0.114
					b	4.827	0.456	8.37	8.27	0.114
					c	5.139	0.579	6.55	5.30	0.128
1.27×10^{10}	119	287	0.77	2.38	t	5.077	0.637	6.29	4.85	0.129
					b	5.221	0.518	6.89	5.91	0.127
					c	5.073	0.605	6.48	5.15	0.127
2.44×10^{10}	135	509	0.65	2.38	t	4.973	0.723	6.04	4.37	0.130
					b	5.227	0.492	7.13	6.30	0.126
					c	5.164	0.571	6.57	5.35	0.128
3.07×10^{10}	132	715	0.58	2.38	t	5.033	0.711	6.02	4.35	0.131
					b	5.392	0.439	7.48	6.95	0.127
					c	5.106	0.793	5.66	3.77	0.137
2.75×10^{10}	156	280	0.77	2.84	t	5.045	0.934	5.38	3.27	0.141
					b	5.126	0.753	5.76	3.95	0.136
					c	5.113	0.789	5.66	3.78	0.137
3.18×10^{10}	153	325	0.70	2.84	t	5.046	0.948	5.36	3.22	0.141
					b	5.208	0.646	6.08	4.53	0.133
					c	5.141	0.767	5.70	3.86	0.137
4.00×10^{10}	148	433	0.58	2.84	t	5.062	0.949	5.34	3.20	0.142
					b	5.278	0.592	6.27	4.89	0.133
					c	5.179	0.746	5.72	3.91	0.137
5.30×10^{10}	147	601	0.53	2.84	t	5.075	0.987	5.25	3.06	0.144
					b	5.376	0.535	6.52	5.35	0.132
					c	5.149	1.12	4.99	2.66	0.152
6.97×10^{10}	164	313	0.52	3.36	t	5.096	1.45	4.71	2.16	0.163
					b	5.252	0.800	5.47	3.53	0.142
					c	5.241	1.00	5.06	2.83	0.150
9.56×10^{10}	157	515	0.43	3.36	t	5.163	1.41	4.67	2.14	0.164
					b	5.420	0.646	5.82	4.19	0.140
					c	5.159	1.10	4.99	2.68	0.151
1.10×10^{11}	159	504	0.42	3.36	t	5.085	1.64	4.59	1.95	0.169
					b	5.337	0.677	5.78	4.10	0.139

gravitational acceleration, L is the height of the cell, Δ is the temperature drop across the cell, and ν and κ are the kinematic viscosity and thermal diffusivity, respectively. In the OB case, the fluid properties throughout the cell are the same, thus there is no ambiguity in the definition of Rayleigh number. However, as the fluid properties vary with the temperature across the cell, we shall redefine the Rayleigh number based on the fluid properties of the central region of the cell. Although this choice is arbitrary, it seems most reasonable since the central region occupies the majority of the cell volume. The Rayleigh number can be increased by adjusting the temperature difference Δ, or by changing the fluid properties. As the gas approaches its critical point by either increasing the gas density or decreasing the average temperature, α increases, ν and κ decrease, consequently the Rayleigh number increases. In this experiment, we vary Δ between 50 and 700 mK, but the Rayleigh number spans eight decades, from 10^3 to 10^{12}. However, for too large a gas density or too low a temperature where the gas is close to its critical point, the fluid properties become so sensitive to the temperature variations that their values differ from the top to the bottom plate. Thus the OB approximation breaks down.

Table I gives the fluid properties for various densities and temperatures. The Rayleigh number R and the Nusselt number N are calculated based on the fluid properties in the central region (the Nusselt number is defined as the actual heat flux normalized by the one which would be transported by gas conduction). x is the ratio of the temperature drop of the top boundary layer to that of the bottom boundary layer; it will be the center topic of this paper. The fifth column is the gas density ρ, which is calculated from the equilibrium pressure and temperature. The cell is isolated after the pressure has been measured. The cell, with a given gas density, may be operated at different average temperatures. Since the central region occupies most of the cell volume, the density there should be very close to the density measured at equilibrium. The fluid properties α, ν, κ, and χ (the thermal conductivity) are computed correspondingly from the density ρ and T_c, where T_c is the central region temperature. The pressure is calculated only from the central region temperature and density, but should be the same throughout the cell. From the average temperature T_t of the top boundary layer and the pressure, the corresponding physical constants α_t, ν_t, κ_t, and χ_t can be calculated. The same calculation can be done for the bottom boundary layer. Note that the subscripts t and b are for top and bottom boundary layer, respectively, while those variables with the subscript c or without any subscript are for the central region.

In the central region, the heat is dominantly transported by convection, while in the top and bottom boundary layers where the velocity tends to zero, the heat is transported by conduction. Since conduction is much more resistive than convection, the total temperature drop across the cell Δ is applied only across the two boundary layers, the central region is isothermal (essentially a thermal short circuit):

$$\Delta=\Delta_t+\Delta_b \ , \tag{2}$$

where Δ_t and Δ_b are the temperature drop across the top and bottom boundary layers, respectively. Δ_t is calculated from the difference of the top-plate and the central region temperatures, while T_t is from the average of the two. Δ_b and T_b are calculated similarly. In the aspect-ratio-1 cell, the temperature profile of the boundary layer has been measured[12] indirectly by varying the Rayleigh number to change the relative position of a fixed bolometer near the bottom plate. In a convection experiment with water, Zocchi, Moses, and Libchaber have measured[15] directly the temperature profile of the convection cell at $R=10^9$ with a moving bolometer. Both results indicate that there are two well-defined boundary layers, which bear all the temperature drop across the cell with a constant gradient.

The temperatures of the top and bottom plates are measured with the thermometers which are fixed in the plates. To measure the central region temperature, a bolometer is positioned at the center of the cell. The bolometer is an arsenic-doped silicon cube of 0.2 mm, which was originally made by NASA for astrophysics observation.[16,17] At 5 K, its typical resistance is around 1 kΩ, and the sensitivity is about 2 mK/Ω. Principally, the central region temperature has to be computed as the average over the whole cross section of the cell, but this is impractical experimentally. In soft turbulence,[11] since there are many independent large-scale structures, our previous study in an aspect-ratio-1 cell shows[18] that the time-average temperature at different points of the same height can be as large as 30% of Δ. Therefore one point measurement at the center cannot be taken as the central region temperature for soft turbulence. In contrast, for hard turbulence,[18] the central region becomes more homogeneous. The maximum temperature difference of the two points is 5% Δ at the onset of hard turbulence, and the difference decreases with the Rayleigh number monotonically. Thus it is a good approximation to use the center temperature measurement as the central region temperature, especially for large Rayleigh numbers. In this paper, we shall only discuss the hard-turbulence regime.

III. EXPERIMENTAL RESULTS

When the OB approximation is valid, x, the ratio between Δ_t and Δ_b, is 1. However, as the OB approximation breaks down, x departs from 1. Thus x is a quantitative measure of the non-OB effects.

Figure 1 is a plot showing x for different Rayleigh numbers. By changing the density, one can coarsely adjust the Rayleigh number. As shown both in Table I and Fig. 1, the density needed to reach $R=10^{10}$ is not large enough for the fluid properties of the two boundary layers to differ dramatically, consequently x is not very different from 1. The fact that the x value is 0.89 for $R=2\times10^8$, smaller than 1, may come from approximating the central region temperature with one point measurement. This approximation improves as the Rayleigh number increases. However, for $R>10^{10}$, x becomes significantly smaller than 1. Since a specific Rayleigh

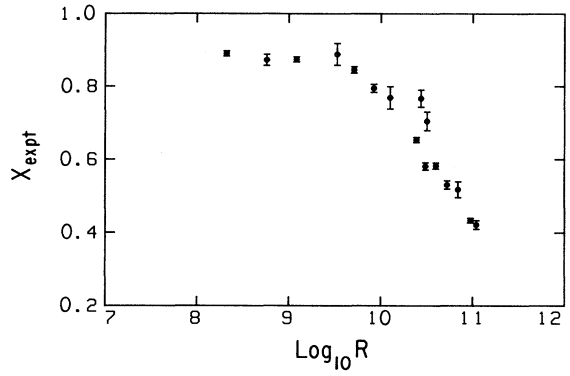

FIG. 1. x_{expt}, the ratio between the measured temperature drops of the top and the bottom boundary layers, is plotted against the Rayleigh number R.

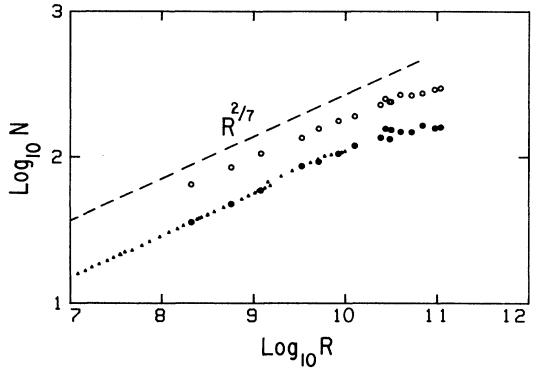

FIG. 3. The log-log plot of the Nusselt number N vs Rayleigh number R. The small dots and the solid circles are the experimental data, but only the solid circles have been analyzed in this paper. The open circles are the theoretical points. The theoretical value has an arbitrary prefactor.

number can be realized with different densities, although they must be close to each other, there is not a one-to-one relation between x and a given Rayleigh number.

As shown in Fig. 1, x can be as small as 0.4, so the two boundary layers are significantly different. Then how does the turbulent temperature fluctuation in the central region feel this difference? Figure 2 shows the histograms of the temperature fluctuation in the central region for $R=1.2\times10^9$, $x=0.87$ and $R=9.6\times10^{10}$, $x=0.43$. They are normalized by their rms temperature fluctuation Δ_c. The normalized histogram for $x=0.43$ has the same shape as that of $x=0.87$, it is symmetric around its mean temperature, despite the big difference between the two boundary layers. These boundary layers adjust themselves somehow so that the fluctuation in the central region is still symmetric around its mean. By the way, the histogram of this large aspect ratio cell is exponential only in certain range, rather than in the full range for the aspect ratio 1 cell.[11] This difference shall be discussed in a future work.

However, non-OB effects may alter the Rayleigh number dependences of the Nusselt number N and rms temperature fluctuation Δ_c normalized by Δ. The solid circles and triangles in Fig. 3 reveal the R dependence of N, whereas the solid circles in Fig. 4 reveal the R dependence of Δ_c/Δ. For $R<10^{10}$, both N and Δ_c/Δ have simple power-law relations with R,N with an exponent 0.29, close to $\frac{2}{7}$, and Δ_c/Δ with an exponent -0.14, close to $-\frac{1}{7}$. These relations have been proposed[12] in a scaling model for hard turbulence, which fits the experimental results for the aspect-ratio-1 cell. However, N and Δ_c/Δ deviate away from the simple power laws for $R>10^{10}$: N seems to saturate with R and Δ_c/Δ decreases faster than with the $-\frac{1}{7}$ power law. The deviation cannot be put into the framework of hard turbulence, unless non-OB effects play a role.

IV. PROPOSED MODELS

Now we try to answer the question of how the cell, with a given density and given top- and bottom-plate temperature, chooses the central region temperature, in

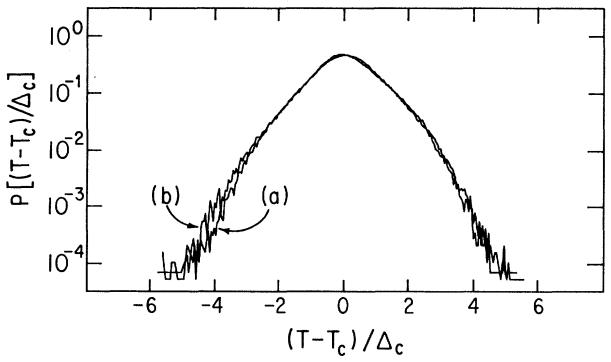

FIG. 2. Comparison of histograms of the temperature fluctuation for (a) $R=1.2\times10^9$, $x=0.87$ and (b) $R=9.6\times10^{10}$, $x=0.43$. The probability for a given temperature is plotted against this temperature. The histograms are all rescaled so that the rms temperature fluctuations coincide.

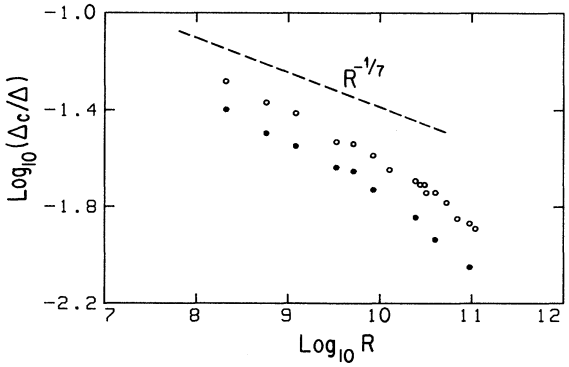

FIG. 4. The log-log plot of Δ_c/Δ vs R. The solid circles are the experimental data, and the open circles are the theoretical points. The theoretical value has an arbitrary prefactor.

other words, how it selects the asymmetry of the two boundary layers, namely x. Furthermore, we try to understand whether non-OB effects have anything to do with the strange Rayleigh number dependences of N and Δ_c/Δ.

Let us consider how many equations we have. We already have Eq. (2), which states that the total temperature drop is across the two boundary layers only. Furthermore, there is the conservation of heat flux. Since the heat is transported purely by conduction in the two boundary layers, then

$$Q=\chi_t\frac{\Delta_t}{\lambda_t}\ , \tag{3a}$$

$$Q=\chi_b\frac{\Delta_b}{\lambda_b}\ , \tag{3b}$$

where Q is the heat flux, χ_t and χ_b are the thermal conductivities for the two boundary layers, and λ_t and λ_b are the two boundary layer thicknesses. From the three equations (2), (3a), and (3b), we are unable to solve for the four unknowns Δ_t, Δ_b, λ_t, and λ_b. One more equation is needed to connect the two boundary layers.

Classically[19,20] the boundary layers are assumed to be marginally stable, therefore their Rayleigh numbers are constant. This implies the equality of the Rayleigh numbers R_t and R_b for the two boundary layers, i.e.,

$$\frac{g\alpha_t\lambda_t^3\Delta_t}{\nu_t\kappa_t}=\frac{g\alpha_b\lambda_b^3\Delta_b}{\nu_b\kappa_b}\ , \tag{4}$$

where the left-hand side is R_t and the right-hand side is R_b. This assumption can be checked from the experimental data. If one substitutes the measured Q, Δ_t, and Δ_b into Eqs. (3a) and (3b), the boundary layer thicknesses λ_t and λ_b can be determined; they are listed in Table II. Thus R_t and R_b can be calculated independently. R_t and R_b have been listed in Table II, and their ratio R_b/R_t is plotted against x in Fig. 5 as open triangles. As x decreases, the ratio diverges away from 1. Therefore this assumption is not corroborated by the experimental results.

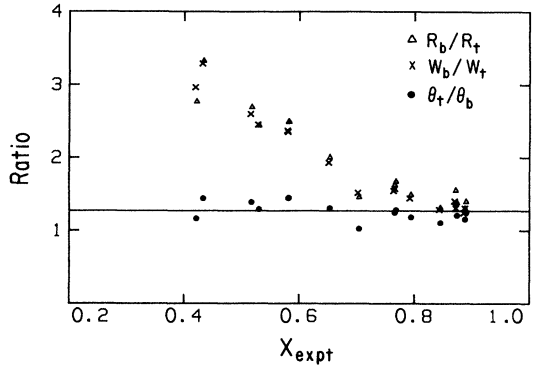

FIG. 5. Ratios between R_b and R_t (open triangles), w_b and w_t (crosses), and Θ_t and Θ_b (solid circles) vs the measured x.

It has been observed that there are many thermals in the central region, which are released from the boundary layers.[15,21,22] Therefore the temperature fluctuations in the central region must be directly related to the properties of the boundary layers. In the scaling model introduced in Ref. 12 (where the OB approximation is assumed), the thermals, with their initial temperature $\Delta/2$, merge into the central region with a velocity w,

$$w=\frac{g\alpha\Delta\lambda^2}{\nu}\ , \tag{5}$$

where this velocity w comes from the balance between the buoyancy force $g\alpha\Delta$ and the viscous force $\nu w/\lambda^2$. Further the temperature fluctuation Δ_c in the central region is the temperature scale Θ of the boundary layers,

$$\Delta_c=\frac{\kappa\nu}{g\alpha\lambda^3}\ , \tag{6}$$

where the right-hand side is Θ. In the OB case, these two

TABLE II. Calculated values of the thickness $\lambda_{t,b}$, the Rayleigh numbers $R_{t,b}$, velocity scales $w_{t,b}$, and temperature scales $\Theta_{t,b}$ of the two boundary layers for different Rayleigh number R.

R	λ_t (μm)	λ_b (μm)	R_t	R_b	w_t (cm/s)	w_b (cm/s)	Θ_t (mK)	Θ_b (mK)	$2S/(S_t+S_b)$
2.10×10^8	390	452	241	337	24.5	32.3	0.698	0.561	0.998
5.75×10^8	291	338	261	406	15.3	21.7	0.282	0.208	0.999
1.21×10^9	235	276	310	428	22.4	29.6	0.536	0.444	1.00
5.13×10^9	148	177	356	466	20.0	26.1	0.461	0.416	1.01
3.35×10^9	163	184	279	362	12.3	15.5	0.253	0.219	0.997
8.42×10^9	128	161	368	548	19.3	28.2	0.441	0.372	1.00
1.27×10^{10}	110	141	343	573	15.1	23.9	0.364	0.283	0.983
2.44×10^{10}	89.8	133	391	783	19.0	37.0	0.515	0.394	0.979
3.07×10^{10}	85.5	143	437	1086	22.2	52.9	0.602	0.416	0.963
2.75×10^{10}	86.1	108	404	656	15.3	23.9	0.301	0.242	1.05
3.18×10^{10}	83.4	112	419	611	16.2	24.8	0.321	0.312	0.976
4.00×10^{10}	77.3	124	400	995	16.6	39.1	0.399	0.275	1.01
5.30×10^{10}	74.1	128	510	1243	21.1	51.9	0.408	0.316	0.943
6.97×10^{10}	70.0	113	447	1202	14.4	37.6	0.239	0.172	0.935
9.56×10^{10}	63.1	124	541	1801	18.3	60.7	0.287	0.199	0.909
1.10×10^{11}	62.5	122	654	1809	20.4	60.8	0.228	0.196	0.897

equations are equivalent. Starting from either, one is able to draw a series of predictions which fit the experimental data of the OB case well.[12] In the non-OB case, although it is not obvious that w_t is the same as w_b, and Θ_t is the same as Θ_b, it is revealing to compare their values in an effort to generalize either Eq. (5) or (6) to the non-OB case. Thus we calculate w_t and w_b, Θ_t and Θ_b, from the fluid properties in Table I and from the boundary layer thickness in Table II. Their values are listed in Table II.

The ratio between w_b and w_t is plotted as crosses in Fig. 5. It diverges away from 1 as x decreases, therefore w_t and w_b do not match. On the other hand, the ratio between Θ_t and Θ_b is plotted as solid circles in Fig. 5. For all the experimental values of x, the ratio remains constant at 1.27 ± 0.13. Compared with the previous two cases (the equality of R and the equality of w), the equality of the two boundary layer temperature scales

$$\Delta_c=\frac{\kappa_t\nu_t}{g\alpha_t\lambda_t^3}=\frac{\kappa_b\nu_b}{g\alpha_b\lambda_b^3} \tag{7}$$

appears to be the best assumption. This assumption is also consistent with the experimental fact that the histogram of the central temperature fluctuations is symmetric even in the strongly non-OB case, i.e., the colder temperature fluctuations is the same as that from the hotter ones. Generalizing Eq. (6), the rms temperature fluctuations in the central region is the same as the two boundary layer temperature scales.

Now that we have Eq. (7), we can write out the expression for x in terms of only the fluid properties. From Eqs. (2), (3a), (3b), and (7), Δ_t and Δ_b can be calculated. Their ratio x is

$$x=\left[\frac{\alpha_b\nu_t\kappa_t}{\alpha_t\nu_b\kappa_b}\right]^{1/3}\frac{\chi_b}{\chi_t}=\frac{S_t}{S_b}\ , \tag{8}$$

where S_t and S_b are defined as $(\nu\kappa/\alpha)^{1/3}(1/\chi)$ for the top and bottom boundary layers. Note that the fluid properties in the two boundary layers are related to x, thus the right-hand side of Eq. (8) is also a function of x. This allows one to uniquely solve for x. Here we use the measured temperature to compute the fluid properties, from which we calculate the theoretical x value from Eq. (8). Figure 6 shows the ratio between the theoretical x value and the experimental x value. The ratio is constant with a value 1.08 ± 0.04, indicating a good agreement between experiment and theory.

Let us point out the uncertainties in the measurement and analysis. First, there are errors in the temperature measurement and the consequence in the fluid properties. The second factor comes from assuming the fluid properties in the boundary layer to be the mean temperature value. Third, there are uncertainties in the McCarty tables and equation, especially close to the critical point. In the error bars of Fig. 6, only the first error is plotted, although the scatter may be due to the second and the third factors as well.

The rms temperature fluctuation Δ_c in the central region has been assumed to be the same as the boundary

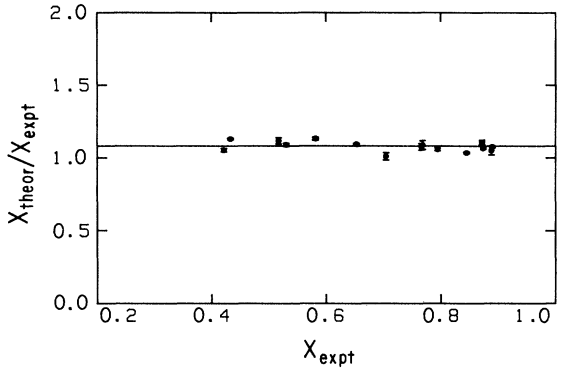

FIG. 6. Ratio between the theoretical and the measured x vs the measured x.

layer temperature scales in Eq. (7). However, in order to express the heat flux Q only in terms of Δ and the fluid properties, a further assumption has to be made about the velocity in the central region. As in Ref. 12, we assume that the thermals in the central region are only driven by the buoyancy force, then

$$V_c=(\alpha gL\Delta_c)^{1/2}\ . \tag{9}$$

The heat flux is

$$Q=C_p\rho\Delta_c V_c\ . \tag{10}$$

Combining Eqs. (8) and (9), one finds

$$Q=C_p\rho(\alpha gL)^{1/2}\Delta_c^{3/2}\ . \tag{11}$$

Here the fluid properties are those of the central region of the cell. From Eqs. (2), (3a), (3b), and (7), λ_t and λ_b can be expressed in terms of Q, Δ, and the fluid properties. Then combining Eq. (7) with (11), the heat flux Q is expressed as

$$Q=\chi\frac{\Delta}{L}\left[\frac{g\alpha L^3\Delta}{\nu\kappa}\right]^{2/7}\left[\frac{\kappa}{\nu}\right]^{1/7}\left[\frac{S}{S_t+S_b}\right]^{9/7}\ , \tag{12}$$

or

$$N=R^{2/7}P^{-1/7}\left[\frac{S}{S_t+S_b}\right]^{9/7}\ , \tag{13}$$

and the temperature fluctuation is

$$\frac{\Delta_c}{\Delta}=R^{-1/7}P^{-3/7}\left[\frac{S}{S_t+S_b}\right]^{6/7}\ , \tag{14}$$

where R and P are the Rayleigh number and Prandtl number ($P=\nu/\kappa$) based on the fluid properties of the central region. For small non-OB effects, $(S_t+S_b)/2$ is close to S, thus the relations between N and R, and between Δ_c/Δ and R are the same as those of the ideal OB case. However, when the non-OB effects are so strong that $(S_t+S_b)/2$ becomes different from S, then both N and Δ_c/Δ depart from the simple power laws. The ratio $2S/(S_t+S_b)$ is listed in Table II. The theoretical Nusselt number is plotted in Fig. 3 as open circles to compare

with the experimental data. One can see that besides the power-law region for $R < 10^{10}$, the theoretical Nusselt numbers change in the same way as the experimental data for $R > 10^{10}$. The theoretical Δ_c/Δ is compared to the experimental one in Fig. 4, with good agreement.

V. CONCLUSION

The assumption that the temperature scales of the two boundary layers are the same is verified experimentally. It is consistent with the observation that the histogram of the central region fluctuation is symmetric even in the strongly non-OB case. This assumption allows us to calculate the ratio of the temperature drops across the two boundaries, and compare it with the measurement. If the velocity in the central region is assumed to be a free-fall velocity, the heat flux and the rms of the temperature fluctuation can be further computed. The agreement is good between the experiments and theory. The scatter of the results may come from the errors in the temperature measurements, the apparent crude approximation about the fluid properties of the boundary layers, and the uncertainties in the fluid properties themselves. All of the above discussion is about hard turbulence, where the large-scale flow is not important in the central region.

ACKNOWLEDGMENTS

We thank M. Sano for helping in all aspects of the experiment, S. Thomae for stimulating discussions, Professor Hilderbrand of the Astrophysics Department for providing us with the bolometers, and A. Simon for revising the manuscript. Special thanks should go to Professor Kadanoff for his guidance in all phases of the work. This research has been supported by the National Science Foundation under Contract No. DMR 8722714.

[1]A. Oberbeck, Ann. Phys. Chem. **7**, 271 (1879).
[2]J. Boussinesq, *Theorie Analytique de la Chaleur* (Gauthier-Villars, Paris, 1903), Vol. 2.
[3]E. L. Koschmieder, Beitr. Phys. Atmos. **39**, 1 (1966).
[4]F. H. Busse, J. Fluid Mech. **30**, 625 (1967).
[5]C. Q. Hoard, C. R. Robertson, and A. Acrivos, Int. J. Heat Mass Transfer **13**, 849 (1970).
[6]E. F. C. Somerscales and T. S. Dougherty, J. Fluid Mech. **42**, 755 (1970).
[7]F. M. Richter, J. Fluid Mech. **89**, 553 (1978).
[8]M. Dubois, P. Berge, and J. Wesfreid, J. Phys. (Paris) **39**, 1253 (1978).
[9]G. Ahlers, J. Fluid Mech. **98**, 137 (1980).
[10]R. W. Walden and G. Ahlers, J. Fluid Mech. **109**, 89 (1981).
[11]F. Heslot, B. Castaing, and A. Libchaber, Phys. Rev. A **36**, 5870 (1987).
[12]B. Castaing, G. Gunaratne, F. Heslot, L. Kadanoff, A. Libchaber, S. Thomae, X. Z. Wu, S. Zaleski, and G. Zanetti, J. Fluid Mech. **204**, 1 (1989).
[13]R. D. McCarty, Natl. Bur. Stand. (U.S.) Tech. Note **631**, (1972).
[14]R. D. McCarty, J. Phys. Chem. Ref. Data **2**, 923 (1973).
[15]G. Zocchi, E. Moses, and A. Libchaber, Physica A **166**, 387 (1990).
[16]A. E. Lange, E. Kreysa, S. E. McBride, and P. L. Richards, Int. J. Infrared Millimeter Waves **4**, 689 (1983).
[17]J. C. Mather, Appl. Opt. **21**, 1125 (1982).
[18]M. Sano, X. Z. Wu, and A. Libchaber, Phys. Rev. A **40**, 6421 (1989).
[19]W. V. R. Malkus, Proc. R. Soc. London Ser. A **225**, 196 (1954).
[20]L. N. Howard, in *Proceedings of 11th International Congress of Applied Mechanics, Munich, 1966,* edited by Henry Goertler (Springer, Berlin, 1966), p. 1109.
[21]T. Y. Chu and R. J. Goldstein, J. Fluid Mech. **60**, 141 (1973).
[22]H. Tanaka and H. Miyata, Int. J. Heat Mass Transfer **23**, 738 (1980).